



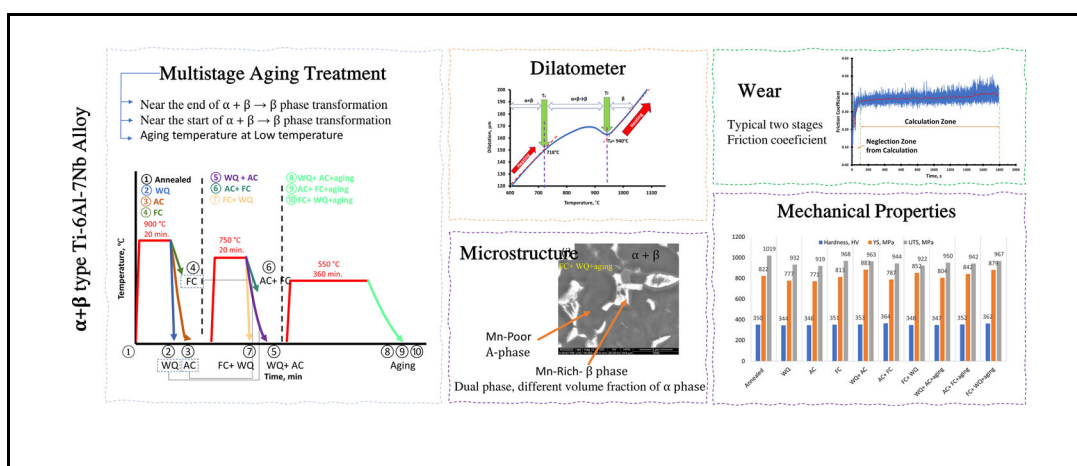
ORIGINAL RESEARCH ARTICLE

Effects of Multistage Aging Treatment on the Microstructure and Mechanical Properties of $\alpha + \beta$ -Type Ti-6Al-7Nb Alloy

Ahmed H. Awad , Shima El-Hadad, Mostafa Ahmed, and Ramadan N. Elshaer

Submitted: 11 July 2023 / Revised: 12 August 2023 / Accepted: 20 September 2023 / Published online: 30 October 2023

The influence of multistage heat treatments on the microstructure and mechanical properties of Ti-6Al-7Nb alloy used for functional structures was systematically studied. Cast Ti-6Al-7Nb alloy samples were subjected to hot forging, annealing, and multiple stages of heat treatments. The relationship between volume fraction of α -phase and the mechanical properties was investigated. Herein, multiple heat treatment steps were selected based on the dilatometric analysis, at the end of the beta transformation and the start of the beta transformation, followed by aging at low temperature, i.e., 500 °C. A higher volume fraction of α -phase leads to higher strength but lower ductility. The yield, ultimate tensile strengths, and ductility of the annealed alloy are 822 MPa, 1019 MPa, and 10%, respectively. The corresponding values for the alloy treated at 900 °C followed by WQ are 777 MPa, 932 MPa, and 16%, while the aged alloy has 879 MPa, 967 MPa, and 12%, respectively. A trade-off between strength and ductility was attained. Besides, the microstructural evolution of the studied conditions was also covered in depth. **Graphical Abstract**



Keywords aging treatment, alpha/beta, mechanical properties, microstructure, Ti-6Al-7Nb

1. Introduction

The usage of titanium (Ti) and its alloys has increased due to their magnificent biocompatibility, mechanical properties, and outstanding corrosion resistance (Ref 1). These alloys are utilized in various design, industry, and science directions (Ref 2).

Behavior of Ti alloys is based on the microstructure content and volume fraction of β (BCC) and α (HCP) phases. The microstructure varies based on the chemical composition of the alloy. Common alloying elements work as β -stabilizers, such as V, Cr, Si, Co, Fe, Mn, Mo, and Nb, whereas O, N, C, and Al are considered α -stabilizers. The α -stabilizer group increases the temperature range of the α -phase, whereas β -stabilizing elements lower the temperatures of β -phase zone. Nb is one of the major β -stabilizers and has higher biocompatibility than α -stabilizing elements, i.e., Al. In addition, α -type Ti alloys are not heat-treatable, whereas $\alpha + \beta$ - and β -type Ti alloys are heat-

Ahmed H. Awad, Design and Production Department, Faculty of Engineering, Ain Shams University, Cairo 11535, Egypt; Shima El-Hadad and Mostafa Ahmed, Department of Manufacturing Technology, Central Metallurgical Research and Development Institute (CMRDI), El-Tebbin, 87, Helwan, Egypt; and Ramadan N. Elshaer, Mechanical Engineering Department, Tabin Institute for Metallurgical Studies (TIMS), Cairo 11913, Egypt. Contact e-mail: ahmed.awad@eng.asu.edu.eg.

treatable and effectively strengthened by various treatments (Ref 3-6).

Ti-6Al-4V (Ti64) alloy is certainly among the most popular $\alpha + \beta$ -type Ti alloys. Illinois Institute of Technology introduced Ti64 alloy in 1950s in the USA and the alloy was registered with international standards (ASTM F 136) (Ref 7). Moreover, researchers are interested in studying Ti64 alloy due to its high corrosion resistance, fatigue, and specific strength. Different microstructures were developed through different techniques and thermal treatments (Ref 8). The medical community questioned much about using non-biocompatible elements, such as vanadium (*V*). The *V* is toxic in both oxide and elemental forms, and considerable efforts have been made to establish another alloy for biomedical applications. A Ti-6Al-7Nb alloy was introduced to defeat the disadvantages of available biomaterials and standardized in (ASTM F1295) international standard. This alloy was essentially proposed for dental and surgical fields, considering niobium (Nb) as a biocompatible element and also β -stabilizing element that can be used to harden the alloy upon thermal treatments. However, after proofing the neurotoxic effect of Al (Ref 5), it was recommended that Ti-6Al-7Nb is better to be used for structural applications similar to Ti-6Al-4V. Some of the recent studies were therefore concerned with improving the mechanical properties of this alloy (Ref 7, 9).

The properties of $\alpha + \beta$ -type Ti alloys specifically depend on the volume fraction and morphology of the constituting phases (α and β). These parameters are affected mainly by alloying elements, processing, and heat treatment processes. In the literature (Ref 9, 10), the phase content is based on treatment temperature, time, and quenching medium. Applying solution treatment for Ti alloys below, the β transus temperature resulted in bimodal microstructures that contain equiaxed α (primary α) in a lamellar matrix ($\alpha + \beta$) (Ref 11). The features of microstructure strongly affect the performance of the alloys, whereas the strength and ductility can be positively influenced by introducing fine-scale microstructures. However, fatigue resistance and creep crack growth can be increased by presenting coarse microstructure. Lamellar microstructures often resist fatigue and creep crack growth and show high fracture toughness, while equiaxed microstructures so often have high fatigue strength and ductility. Bimodal microstructures gather the advantages of both equiaxed and lamellar structures; they demonstrate a coordinated property profile (Ref 12).

Ashida et al. (Ref 13) investigated the microstructure evolution and mechanical properties of Ti-6Al-7Nb alloy produced by a high-pressure torsion process and subsequent heat treatment. The authors succeeded in achieving a grain size of less than 100 nm. The high ductility of 22% and tensile strength of 1280 MPa were achieved because of the duplex microstructure and α' needlelike shape. Li et al. (Ref 14) investigated alloying Ti-6Al-7Nb with (0-20 wt.%) Zr and process with hot rolling. The DSC results revealed that adding 20 wt.% Zr reduced the β transus temperature from 956 to 790 °C, since Zr is a β -stabilizing element. The yield, tensile strength, and ductility improved by adding Zr to 858, 1160 MPa, and 9.5%, respectively, for Ti-6Al-7Nb-15Zr alloy, compared to 810, 1331 MPa, and 11.6%, respectively, for Ti-6Al-7Nb-20Zr alloy. The authors claimed the enhancement of tensile properties to the solid-solution strengthening resulting

from Zr addition and metastable phases introduced by the high-temperature transformation.

Xu et al. (Ref 15) investigated the microstructure and mechanical properties of Ti-6Al-7Nb alloy manufactured by laser powder bed fusion. The as-built sample showed a yield, tensile strength, and ductility of 1082, 1160 MPa, and 9.7%, respectively, compared to 871, 940 MPa, and 11.5%, respectively, for the solution-treated sample at 1055 °C for 1 h, cooled in air, and subjected to subsequent aging at 540 °C for 4 h and air cooling. The heat treatment made the alloy suitable to mate with the ISO 5832-3 standard requirement, which quoted that a minimum of 10% ductility must be obtained.

Kalienko et al. (Ref 16) assessed the thermal stability of Ti-6Al-7Nb and Ti-6Al-2Sn-4Zr-2Mo-0.1Si alloys. After heating at 700 °C for 100 h, both alloys formed an oxide layer with a thickness of 46 and 44 μm in Ti-6Al-7Nb and Ti-6Al-2Sn-4Zr-2Mo-0.1Si, respectively. The authors claimed the lower oxygen content at the oxide layer to the presence of niobium.

The current research emerges principally from surveying the literature, where a special attention is given to Ti-6Al-7Nb alloy. However, there is still a gap in the effect of multi-step aging treatments on the microstructure and mechanical properties of this alloy. In the ongoing experiments, Ti-6Al-7Nb alloy was subjected to a novel heat treatment cycle to study its effect on the microstructure and mechanical behavior.

2. Experimental Work

2.1 Material

The forged Ti-6Al-7Nb (wt.%) alloy was received as rods of 8 mm from BAOJI XUHE Titanium Metal Co., Ltd. The rods were prepared from a 500 kg ingot produced under vacuum in an induction furnace. The chemical composition after forging was obtained and is summarized in Table 1.

2.2 Dilatometric Study

The phase transformation of Ti-6Al-7Nb alloy during heating and cooling was detected using a controlled vertical pushrod dilatometer (LINSEIS DIL L76 instrument). The specimen was cut using a wire electrical discharge machine (EDM) with a diameter of 5 mm and a length of 20 mm. After that, the specimen was heated with a heating rate of 10 °C/min up to 1100 °C before cooling to room temperature. Standard specimens of alumina and Al were used to determine the apparatus behavior and to calibrate the device. A WIN-DIL software was installed to track the length variation as a temperature function. Finally, the $\alpha + \beta \leftrightarrow \beta$ phase transformation temperatures were determined from the first derivative between the length and temperature (Fig. 1).

The variation in the length of the annealed Ti-6Al-7Nb alloy was detected during linear heating and cooling with a heating and cooling rate of 10 °C/min up to 1100 °C. The results of all variations of thermal expansion and contraction are shown in Fig. 2. The curve shows a deviation from linearity in the heating cycle, while no deviation was detected in the cooling cycle. The main parameter extracted from the dilatometry is the β transus temperature according to the technique described in

Table 1 Chemical composition of forged Ti-6Al-7Nb alloy

Nominal composition	Average chemical composition, wt.%							
	Al	Nb	Fe	C	N	H	O	Ti
Ti-6Al-7Nb	6.1	6.8	0.02	0.01	0.01	0.002	0.14	Bal.

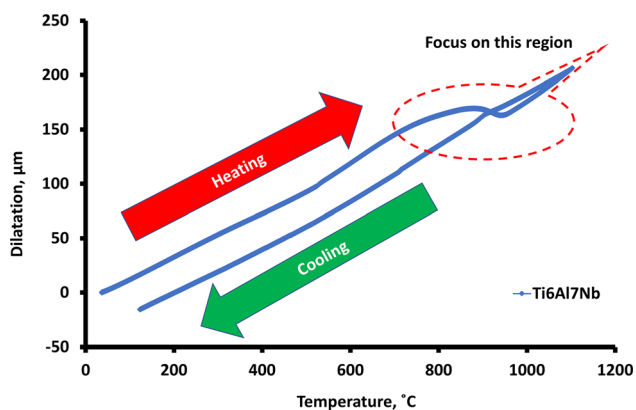


Fig. 1 Variation in length as a function of temperature for Ti-6Al-7Nb alloy

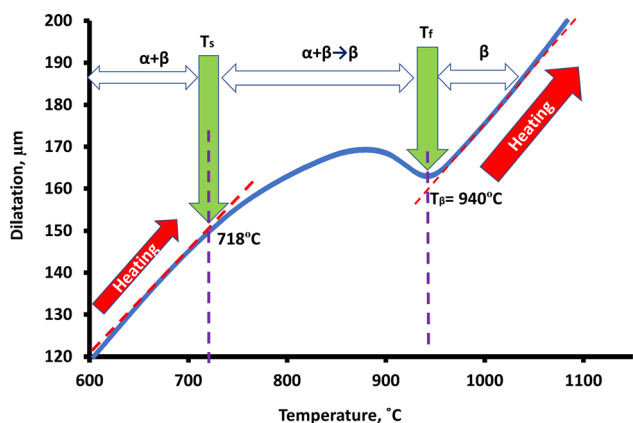


Fig. 2 Close look at the starting and finishing temperatures of $\alpha + \beta \rightarrow \beta$ phase transformation in the heating cycle for Ti-6Al-7Nb alloy

the ASTM standard (Ref 17). In utilizing this method, the β transus temperature corresponds to the lowest temperature not fitting with the straight line drawn during the expansion of the alloy (Ref 18).

The area of focus in the dilatation test, marked in Fig. 2, was plotted separately in Fig. 3. At the initial stage of heating, the annealed ($\alpha + \beta$ -type) Ti-6Al-7Nb alloy dilated linearly due to the expansion of α and β phases crystal lattices at linear heating. When heated to 718 °C, schematically denoted by a vertical line and T_s in Fig. 3, the annealed Ti-6Al-7Nb alloy began to contract with a decrement slope caused by a negative dilatation influence of the α phase. With the proceeding of $\alpha + \beta \rightarrow \beta$ transformation, the dilatation curve continued to

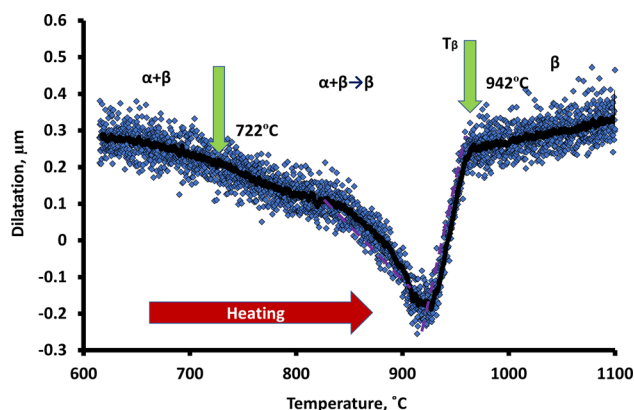


Fig. 3 First derivative for dilatometric heating curve for Ti-6Al-7Nb alloy

decrease and reached a minimum temperature of 940 °C (β transus) and till the end of the transformation, schematically denoted by a vertical line and T_f in Fig. 3. After that, the β phase dilated linearly up to 1100 °C. Several pieces of the literature reported the β transus of Ti-6Al-7Nb alloy. Li et al. (Ref 14) reported the β transus by DSC test of 956 °C for as cast Ti-6Al-7Nb alloy. Bolzoni et al. (Ref 19) reported a β -transus temperature of 1010 °C from the DTA curve applied on Ti-6Al-7Nb powders.

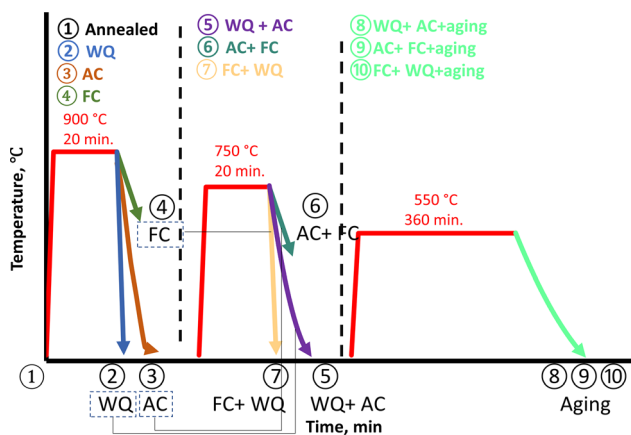
Further information can be found in the first derivative of thermal expansion, which clearly detects the linearity variation and converts it to a peak. This method provides an accurate and objective way to get the start and finish transformation temperatures (i.e., $\alpha + \beta \rightarrow \beta$). The start and end transforming temperatures using the first derivative method were extracted at 722 °C and 942 °C, respectively, which are close to the values acquired in the dilatometry heating curve (718 °C and 940 °C).

2.3 Treatment Schemes

The as-received samples of Ti-6Al-7Nb alloy were subjected to an annealing process at 550 °C for 2 h in a Nabertherm tube furnace R70/9 under an argon atmosphere followed by furnace cooling. This annealing aims to relieve the residual stresses from the previous forging without harmfully affecting the properties of the Ti alloy (Ref 20). After that, the samples were subjected to multiple heat treatment tracks, all of which are summarized in Table 2. The selection of the 900 °C in heat treatment was based on promoting high diffusion and high thermal energy near the end of $\alpha + \beta \rightarrow \beta$ phase transformation detected from dilatometry results, just below the β transus temperature (Fig. 2 and 3). Likewise, the temperature of 750 °C was selected to be near the start of $\alpha + \beta \rightarrow \beta$ phase transformation to see the behavior of the material just at the

Table 2 Sample number, its heat treatment, and the abbreviation of the studied conditions

Number	Heat treatment	Abbreviation
1	Annealed	Annealed
2	900 °C/20 min → WQ to room temp.	WQ
3	900 °C/20 min → AC to room temp.	AC
4	900 °C/20 min → FC to room temp.	FC
5	900 °C/20 min → WQ to room temp. + 750 °C/20 min → AC to room temp.	WQ + AC
6	900 °C/20 min → AC to room temp. + 750 °C/20 min → FC to room temp.	AC + FC
7	900 °C/20 min → FC to room temp. + 750 °C/20 min → WQ to room temp.	FC + WQ
8	900 °C/20 min → WQ to room temp. + 750 °C/20 min → AC to room temp. + 550 °C/360 min → AC to room temp.	WQ + AC + aging
9	900 °C/20 min → AC to room temp. + 750 °C/20 min → FC to room temp. + 550 °C/360 min → AC to room temp.	AC + FC + aging
10	900 °C/20 min → FC to room temp. + 750 °C/20 min → WQ to room temp. + 550 °C/360 min → AC to room temp.	FC + WQ + aging

**Fig. 4** Schematic for the heat treatment cycle for the studied conditions of Ti-6Al-7Nb alloy

beginning of the transformation, just above the start of β transformation. The aging temperature of 500 °C was chosen to avoid the formation of β' and/or isothermal ω phases (Ref 21, 22). First, the samples were treated in a Nabertherm tube furnace R70/9 under inert gas at 900 °C for 20 min, followed by water quenching (WQ), air cooling (AC), and furnace cooling (FC) to the room temperature. After that, all previous conditions were subjected to another step ordering heat treatment at 750 °C for 20 min, followed by AC, FC, and WQ, respectively, reaching the room temperature (i.e., WQ + AC, AC + FC, and FC + WQ). Finally, all previous conditions were subjected to aging treatment at 550 °C for 360 min, followed by AC (i.e., WQ + AC + aging, AC + FC + aging, and FC + WQ + aging). All specimens with several heat treatment processes are shown in Fig. 4.

2.4 Microstructural Investigations

The microstructure was attained after grinding, polishing, and etching with a Kroll solution ($\text{H}_2\text{O}:\text{HNO}_3:\text{HF}$ —67:30:3). The samples were investigated using a scanning electron

microscopy (JSM-5410) equipped with an energy-dispersive x-ray analysis (INCA PENTAFET X₃ EDS Detector).

The crystal structure of thermally treated Ti-6Al-7Nb alloy was studied through the x-ray diffraction (XRD) using a D8 DISCOVER BRUCKER diffractometer equipped with a Cu K α radiation source with a wavelength of 0.15418 nm, operated at a current of 40 and an accelerated voltage of 40 kV 40 mA. The diffractogram of thermally treated Ti-6Al-7Nb alloy was indicated with ICDD PDF 03-065-7479, ICDD PDF-2 01-089-5009, and ICDD PDF 00-001-1198.

2.5 Mechanical Testing

The mechanical properties of thermally treated Ti-6Al-7Nb alloy were evaluated by tension and hardness tests. The yield strength (YS), ultimate tensile strength (UTS), and elongation (% $\Delta l/l$) were determined at room temperature on dog-bone-shaped specimens with a gauge length of 28 mm and a diameter of 5 mm using a universal testing machine (WDW-300) with a cross-speed of 5 mm/min. The hardness values of five indentations on polished specimens were obtained by Vickers Härteprüfergerät Otto Wolpert Testor HT2001 hardness tester machine using a load of 10 kg for 15 s. at room temperature. Sliding wear tests were performed for thermally treated Ti-6Al-7Nb alloy on a pin-on-disk-type machine (T-01 M) tribometer, using a counter disk made of hard steel (65 HRC), while the pin was the specimen test with dimensions of (7 × 6 × 6 mm). The wear test machine was adjusted to a load of 80 N, a speed of 500 rpm, a sliding distance of 1500 m, a sliding velocity of 0.837 m/s, and a wear track radius of 16 mm. The specimen was ground and cleaned before the test, and the debris was removed after the test for accurate measurements. The test was performed on three specimens at room temperature, where the temperature and the friction coefficient were monitored and recorded during the test. The roughness of the worn surface was studied using a ZEISS Axioscope and imager analyzer.

3. Results and Discussion

3.1 Microstructural Investigation

To discover the effect of the heat treatment cycle on the phase stability of Ti-6Al-7Nb alloy, low- and high-magnification secondary electron SEM images of all studied conditions were captured, as shown in Fig. 5 and 6, respectively. The average volume fraction of α and β phases was calculated using ImageJ 1.53e software. The heat treatment cycle for Ti-6Al-7Nb alloy was given as 900 °C, followed by WQ, AC, and FC.

Subsequent treatment was performed at 750 °C, followed by WQ, AC, and FC. Finally, aging treatment was applied at 500 °C, followed by AC.

The SEM images of numerous heat treatment conditions showed similar microstructures, except for the volume fraction and the distribution of the primary α phase. The SEM images show the dominant recrystallized α phase (indicated by a dark area in the SEM images) alongside the transformed β phase (indicated by a light area in the SEM images). The microstructure of annealed Ti-6Al-7Nb alloy (Fig. 5(a)) shows a fine α phase with a random orientation, and its volume fraction is

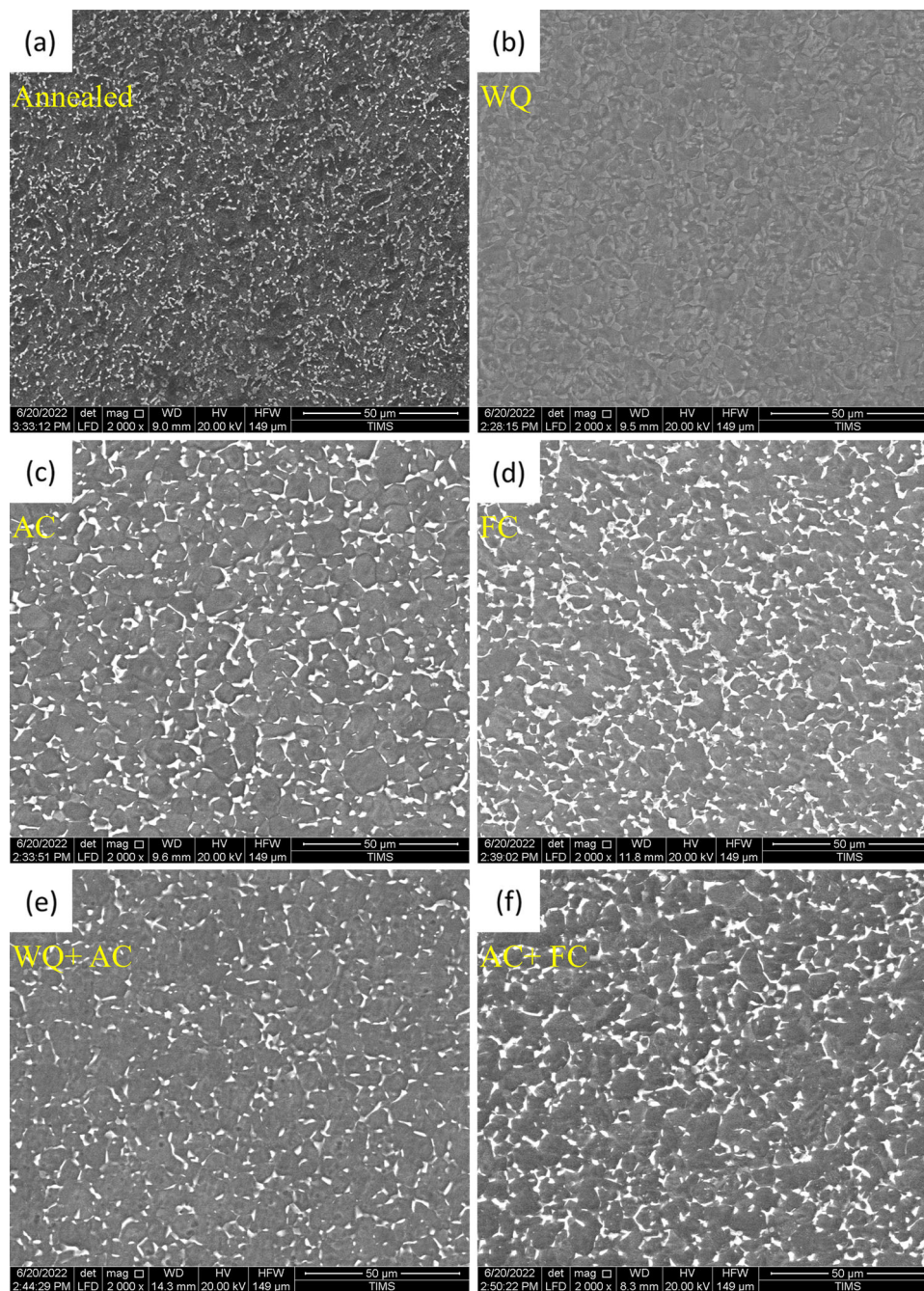


Fig. 5 Low-magnification secondary electron SEM images of (a) annealed, (b) WQ, (c) AC, (d) FC, (e) WQ + AC, (f) AC + FC, (g) FC + WQ, (h) WQ + AC + aging, (i) AC + FC + aging, and (j) FC + WQ + aging Ti-6Al-7Nb alloy

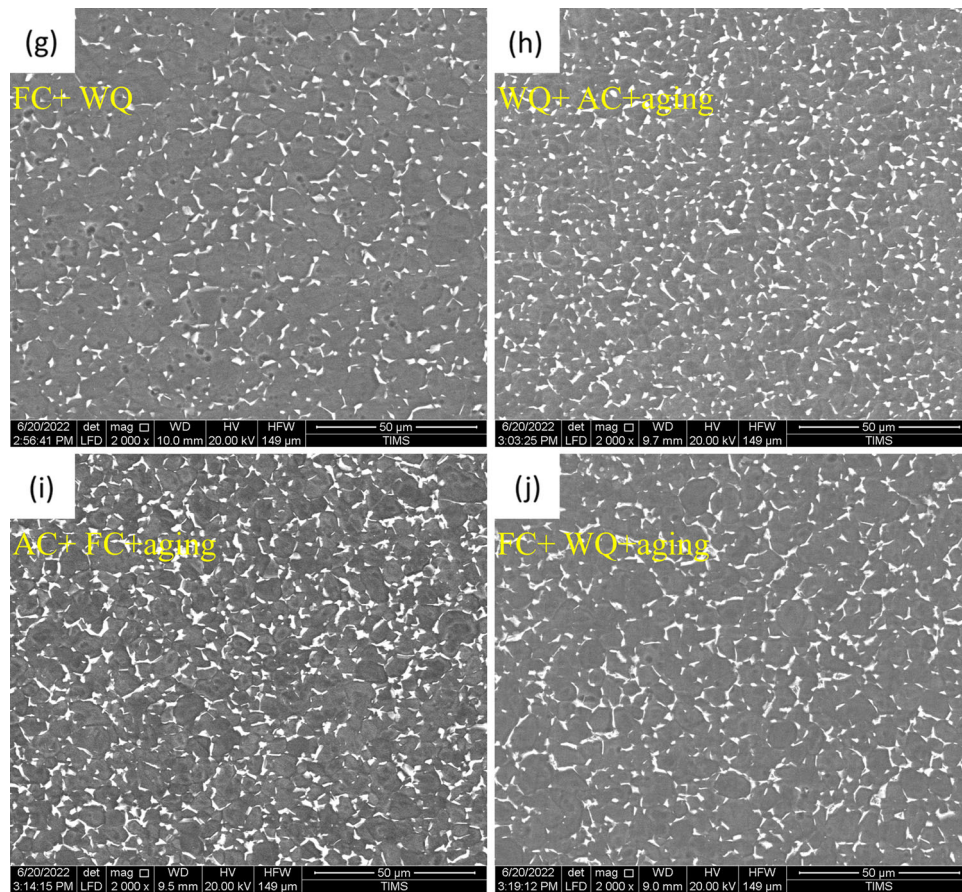


Fig. 5 continued

about 84.7 %, which may reflect the strength of the alloy. The solution treatment at 900 °C for 20 min. followed by WQ started the transformation, and the subsequent fast cooling helped to freeze the microstructure. At the same time, the amount of α phase seems to be lower, about 61.2%, and coarser, helping to decrease the strength and increase the ductility. However, in the case of solution treatment at 900 °C for 20 min followed by AC and FC, presented in Fig. 5(c) and (d), the microstructure shows recrystallized, randomly oriented, and coarse α phase alongside the transformed β phase, where the volume fraction is about 84.3 and 81.1% for AC and FC conditions, respectively.

Furthermore, in the subsequent treatment at 750 °C for 20 min, the amount of primary α phase seems to be higher (in all conditions) with a volume fraction of 87, 86.4, and 88.6% for WQ + AC, AC + FC, and FC + WQ conditions, respectively. The variation of volume fractions is the main reason for the alloy strength and ductility variation. Further, in aging treatment at a low temperature, 550 °C for 360 min, followed by AC, the microstructure revealed the presence of primary α phase with some fine secondary α phase, indicating the precipitation strengthening during aging. The volume fraction seems to be the same, 86, 83.3, and 86.4% for WQ + AC + aging, AC + FC + aging, and FC + WQ + aging conditions, respectively. However, this may be due to the difficulty of detecting the fine features using ImageJ software.

High-magnification secondary electron SEM images of all conditions were captured and are presented in Fig. 6. In all states, the alloys showed primary α phase and irregular shapes with sharp corners, which may reflect its ductility.

EDX point analysis corresponding to SEM images of Ti-6Al-7Nb alloy was performed to scrutinize the phase elemental distributions. The two phases observed with different colors were analyzed, whereas no other phases were detected. Meanwhile, the EDX spectra showed similar results for all conditions; only one representative condition is presented. The EDX point analysis of AC, AC + FC, and AC + FC + aging conditions for Ti-6Al-7Nb alloy was interpreted as an example of the sequence of heat treatments, as shown in Fig. 7. EDX point analysis identified Al-rich regions most likely in the α phase and Nb-rich regions most likely in the β phase, following the rule of phase stability. Although the distribution of elements in Ti-6Al-7Nb is unclear, the content of Nb in the β phase is high in the beta phase due to diffusion.

The treatment below the β transus temperature of $\alpha + \beta$ -type Ti alloys led to a duplex microstructure containing primary α -phase and transformed β -phase. The volume fraction of both phases was affected mainly by the treatment temperature, and the volume fraction of the transformed β -phase was expected to increase at a higher temperature. Meanwhile, the cooling rate affected the size and shape of the constituted phases. A fast cooling rate was achieved in WQ, and fine grains were

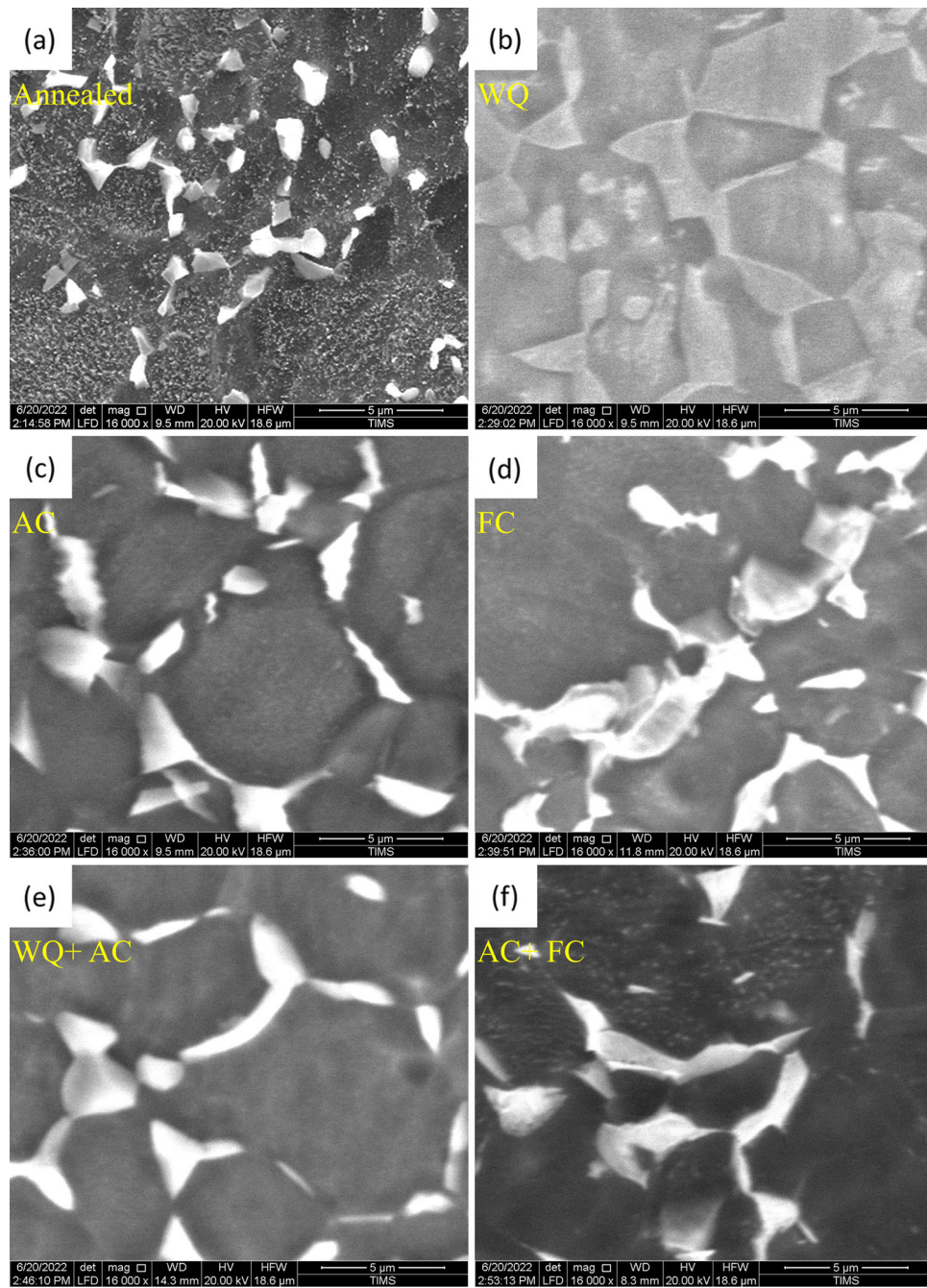


Fig. 6 High-magnification secondary electron SEM images of (a) annealed, (b) WQ, (c) AC, (d) FC, (e) WQ + AC, (f) AC + FC, (g) FC + WQ, (h) WQ + AC + aging, (i) AC + FC + aging, and (j) FC + WQ + aging Ti-6Al-7Nb alloy

produced. However, a slower cooling rate was observed in FC, and coarse grains were produced. An intermediate result was achieved in AC. The results agree with those reported for different treatments on Ti-6Al-4V alloy (Ref 23). There is no significant variation in the chemical composition of different cooling rates, suggesting that the chemical distribution along the phases follows only the phase stability rule.

To further investigate the change in the microstructure because of the heat treatment, XRD patterns of AC, AC + FC,

and AC + FC + aging conditions for Ti-6Al-7Nb alloy are shown in Fig. 8. The relative intensity of the peaks and location of the peaks of α , β , and omega (ω) phases are plotted versus the diffraction angle (2θ).

The peaks of Ti-6Al-7Nb alloy after treatment originated from the α and β phases, which matches well the SEM micrographs. However, a small peak of the ω phase was detected during the AC condition. The ω phase may appear experimentally during the cooling in some Ti alloys (Ref 24).

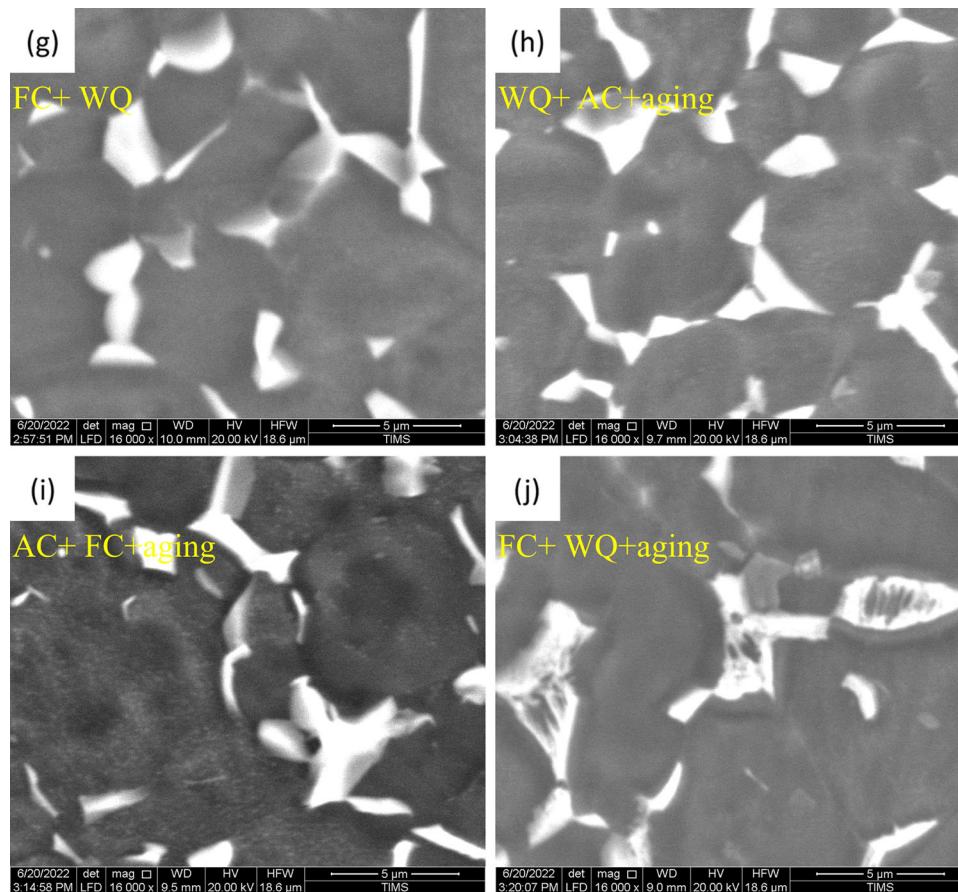


Fig. 6 continued

The main diffraction peaks in 2θ range of 10° - 100° are almost coincident. However, the intensity of some phases reduced and other peaks were introduced. The XRD patterns show that the peaks of α -phase and its volume fraction decreased with solution treatment.

In the annealed condition, a small content of β phase was observed. After the heat treatment near the end of $\alpha + \beta \rightarrow \beta$ phase at 900°C followed by AC, the microstructure and XRD pattern revealed α -phase with traces of β -phase. After subsequent treatment at 750°C followed by FC, AC + FC, a small content of retained β phase was detected (around $2\theta = 36$). However, after aging at 550°C , a fine microstructure consisting of α -phase was obtained compared to AC and AC + FC conditions. According to the SEM images and XRD patterns, at the aging temperature of 550°C , the content of α -phase increases at the expense of the β -phase amount, whatever the solution treatment temperature. The aging succeeded in forming a fine α -phase, which was expected to influence the mechanical properties of the alloy. This observation agreed with the previously reported research on Ti alloys (Ref 25). Earlier works (Ref 26, 27) showed that the ω phase can be observed after treatment in the β -phase zone.

3.2 Mechanical Properties

The results of the hardness test are displayed in Table 3. The results revealed that the heat treatment significantly influenced the volume fraction of each phase and hence the microhardness. The thermal treatment phenomena was the reason for the increased microhardness of the subsurface and surface. In all thermal treatment tracks, WQ resulted in minimum hardness, 344 HV, due to the lowest volume fraction of hard and brittle α -phase. In the case of the FC specimen, a slower cooling rate and higher hardness were obtained, 351 HV. The intermediate-temperature treatment cycle was utilized to make a suitable mixture of α phase and transformed β phase (Ref 26). The intermediate-temperature treatment increased the hardness of the Ti-6Al-7Nb alloy. The highest hardness of (364 HV) was obtained for the aged Ti-6Al-7Nb alloy. Aging treatment at low temperatures, i.e., 500°C , led to fine precipitate strengthening.

Figure 9 shows the representative engineering stress-strain curve produced under selected thermally treated conditions at room temperature for Ti-6Al-7Nb alloy. The tensile test proceeded up to the alloy failure. All thermally treated alloys exhibited the same behavior, yielding 770-890 MPa, ultimately strength at 915-1020 MPa, and 10-16% ductility. The volume fraction of α -phase, hardness, yield, and ultimate tensile strengths for thermally treated Ti-6Al-7Nb alloy were extracted

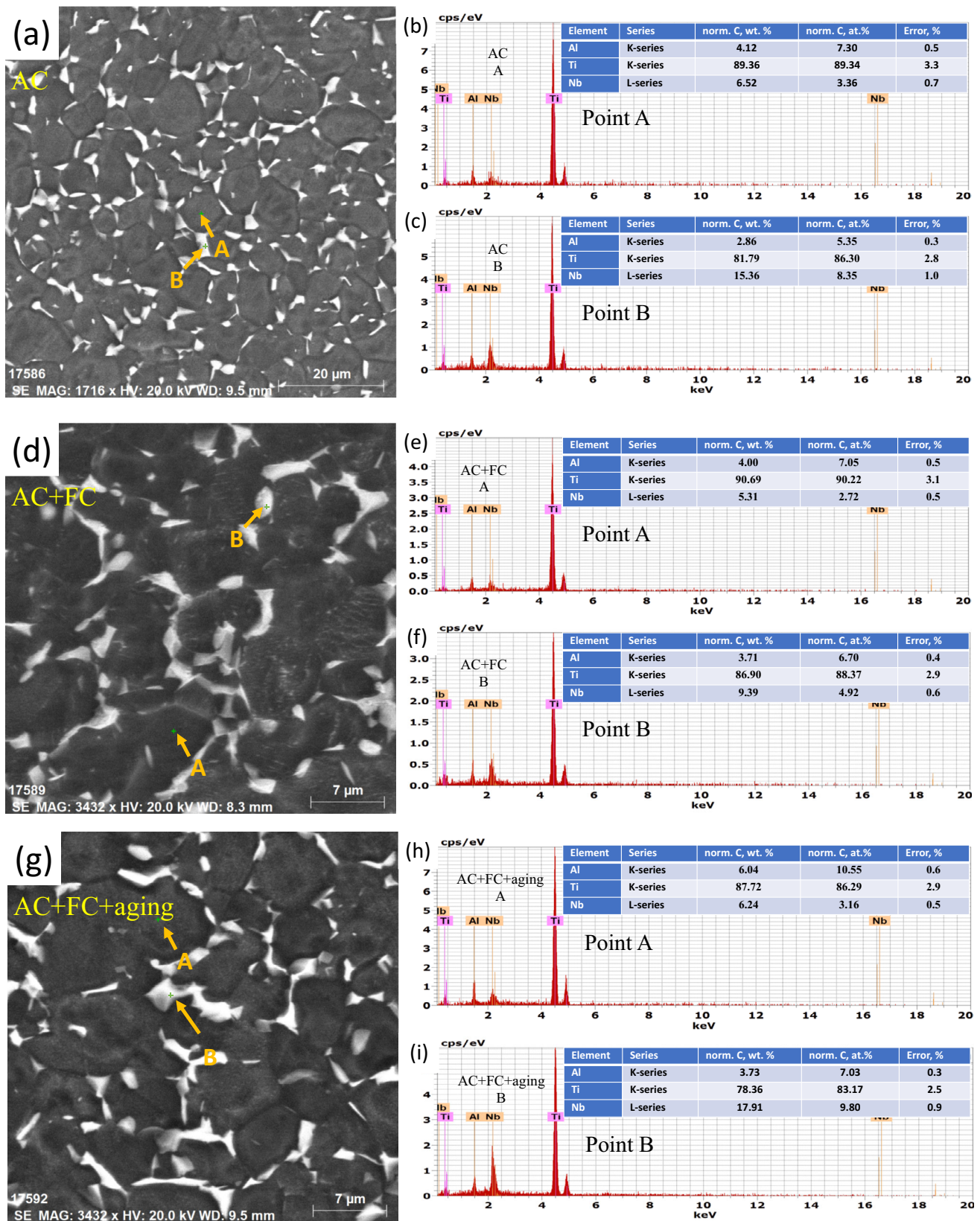


Fig. 7 SEM micrographs of AC, AC + FC, and AC + FC + aging conditions for Ti-6Al-7Nb alloy and the corresponding EDX spectra and quantification of A and B points at each condition

and are summarized in Table 3. The results revealed that the mechanical properties of Ti-6Al-7Nb alloy after treatments can be related to the volume fraction of α -phase.

The annealed Ti-6Al-7Nb alloy showed the highest UTS of 1019 MPa and the lowest ductility of 10%. This can be related to deformation strengthening from the hot forging process since

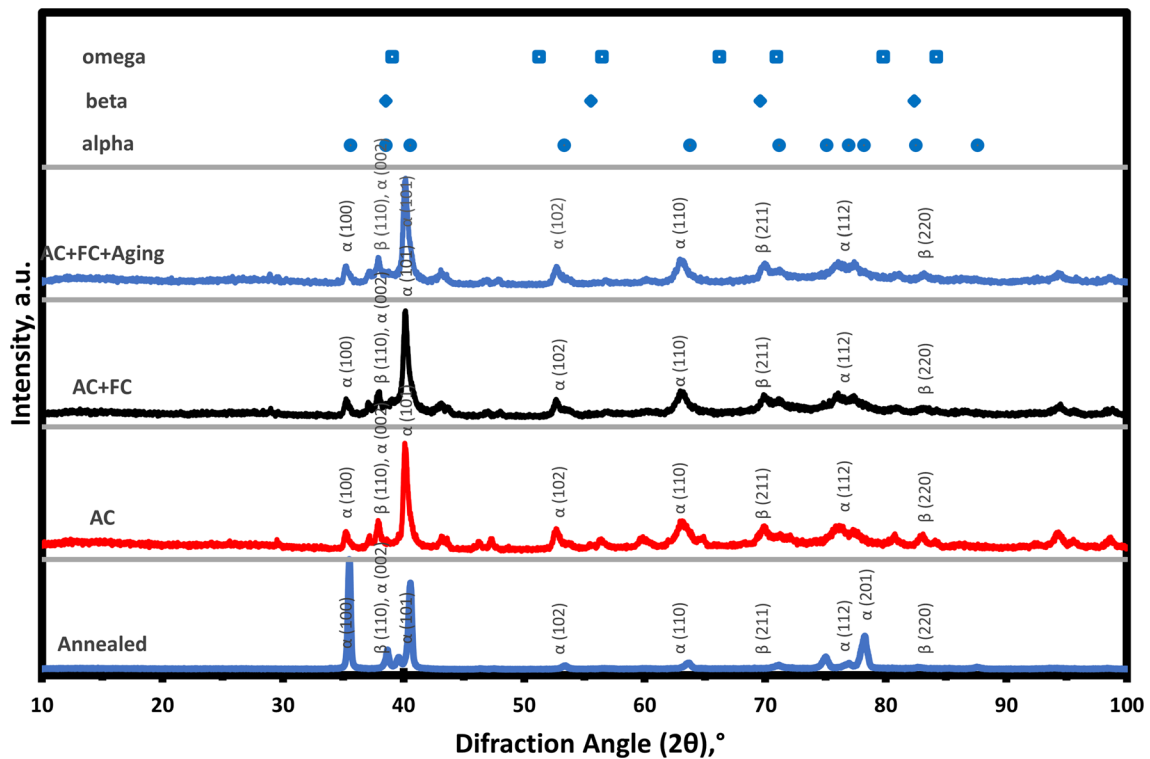


Fig. 8 XRD patterns of AC, AC + FC, and AC + FC + aging conditions for Ti-6Al-7Nb alloy

Table 3 Volume fraction of α -phase, hardness, yield, ultimate tensile strengths, and coefficient of friction for thermally treated Ti-6Al-7Nb alloy.

Conditions	V_{α} %	Hardness, HV	YS, MPa	UTS, MPa	Elongation, %	CoF
Annealed	84.7	350 ± 2	822	1019	10	0.399
WQ	61.2	344 ± 5	777	932	16	0.410
AC	84.3	346 ± 9	771	919	13.5	0.411
FC	81.1	351 ± 4	813	968	13	0.407
WQ + AC	87.0	353 ± 4	883	963	12.5	0.405
AC + FC	86.4	364 ± 3	787	944	13.5	0.380
FC + WQ	88.6	348 ± 4	852	922	12	0.403
WQ + AC + aging	86.0	347 ± 2	804	950	12	0.413
AC + FC + aging	83.3	352 ± 9	842	942	13	0.383
FC + WQ + aging	86.4	362 ± 2	879	967	12	0.388

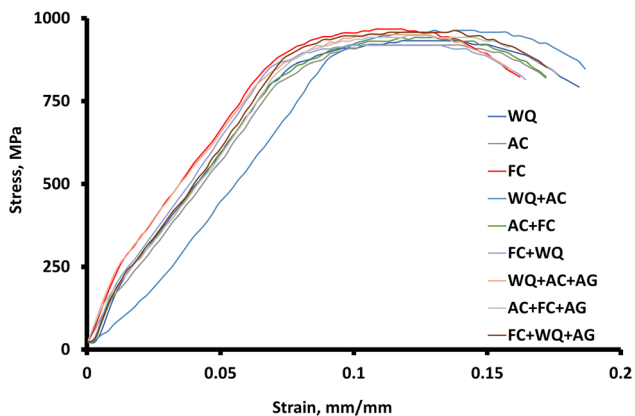


Fig. 9 Engineering stress–strain curve of tensile specimen for thermally treated Ti-6Al-7Nb alloy

the stress relieving process did not alter the mechanical properties. The samples were treated to tailor the mechanical properties of Ti-6Al-7Nb alloy. The WQ Ti-6Al-7Nb alloy exhibited the highest ductility (16%) because the microstructure had the lowest volume fraction of hard α -phase. The α -phase volume fraction can significantly change the alloy's mechanical properties. The morphology and content of every phase are based on the treatment temperature and time. The aging process reduced the ductility of Ti-6Al-7Nb alloy due to the possible formation of brittle ω -phase precipitation (Ref 27). An intermediate thermal treatment was obtained to slightly improve the ductility and YS of the alloy. In almost all aging treatments, aging at 550 °C for 360 min improved the YS and UTS due to forming a small α phase (Fig. 6(i) and (j)), which results in high interfacial strengthening result (Ref 28). The aged alloy at 500 °C showed high yield strengths, 879 MPa, and moderate ductility, 12%, owing to the precipitation

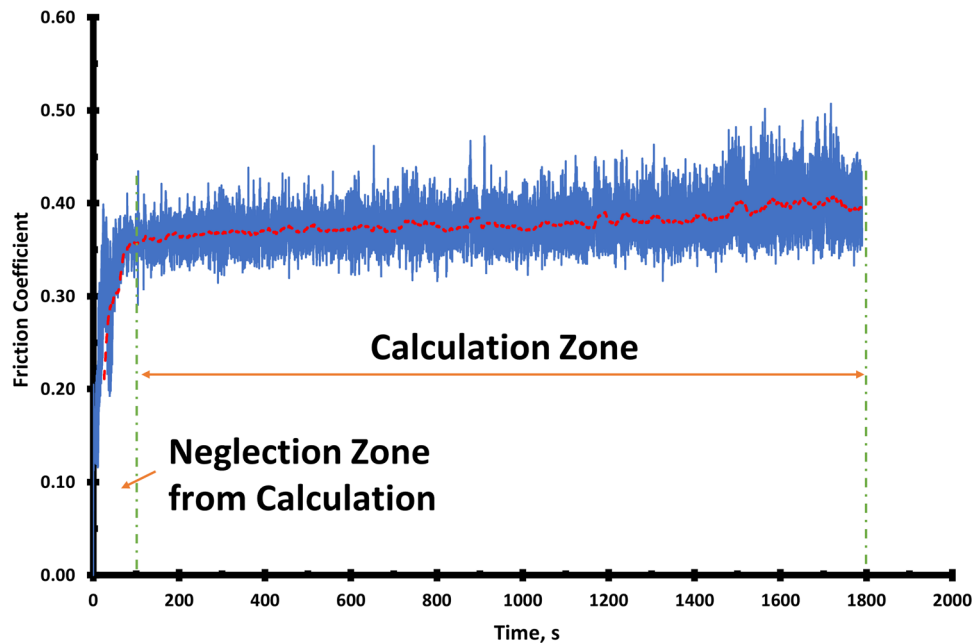


Fig. 10 Representative wear result of a specimen thermally treated Ti-6Al-7Nb alloy

hardening effect. The lowest UTS was 922 MPa for FC + WQ alloy.

Generally, the β phase is softer compared to the α phase. Other factors governed the variation in mechanical properties, such as the amount of alloying elements, the beta stability effect, the size and morphology of secondary phases, the grain size, and residual stresses (Ref 23).

The dependency of thermally treated Ti-6Al-7Nb alloy friction coefficient on the sliding distance is plotted in Fig. 10. The coefficient of friction (CoF) was calculated and is presented in Table 3. The graph analysis was distinguished into two successive regimes or periods of friction. Firstly, the CoF increased rapidly, during which an accommodation period occurred, where either the sample was instilled on the disk or presented the elastic zone, in which, by its end, a plastic deformation occurred (Ref 29). Finally, a stabilization zone for the friction coefficient occurred, during which the average CoF was calculated. Table 3 presents the variation of CoF under different heat treatments. As shown in the table, the change in CoF ranged from 0.38 to 0.413 for all the treatments. It can be observed that the CoF gradually increased as the hardness decreased, which also agrees with the results from the literature (Ref 30, 31). The increment of CoF was due to the higher deformation of the soft and ductile phase in the alloy, in this case, the β phase. It is seen from the table that the CoF displayed a higher value of 0.413, at a hardness of 347 HV, for WQ + AC + aging Ti-6Al-7Nb alloy, compared to a lower value of 0.38, at a hardness of 364 HV, for AC + FC Ti-6Al-7Nb alloy. Even though the volume fraction of the α phase was almost the same, the size of the phase was different. The CoF can be related to the hardness of the material, where hard material is hard to deform plastically during the wear test. The morphological analysis of the worn surface of thermally

treated Ti-6Al-7Nb alloy is shown in Fig. 11. The optical images presented in the figure show evidence of wear tracks detected on all tested specimens. The figures show plastically deformed ridges, grooves, and continuous sliding marks. All the conditions showed almost the same features and a similar wear mechanism. All samples showed parallel grooves along the sliding direction covered by wear debris. Materials with low hardness showed layers with smooth surfaces. The hardness was the most significant parameter affected the CoF, as the hardness was higher, i.e., AC + FC Ti-6Al-7Nb alloy had more hardness than WQ + AC + aging Ti-6Al-7Nb alloy; thus, the depth of abrasive marks was lower; see Fig. 11(f) and (h). Yet, there was no significant variation in wear features of thermally treated Ti-6Al-7Nb alloy.

4. Conclusions

The influence of heat treatment cycles on the microstructure and mechanical properties of Ti-6Al-7Nb alloy with dual phases (α and β) were systematically investigated. The conclusions are as follows:

1. With a lower cooling rate, the volume fraction of α -phase of Ti-6Al-7Nb alloy gradually increased from 81.1 to 86.4%.
2. At high treatment temperatures, i.e., 900 °C, and with a high cooling rate, the volume of transformed β phases became larger, 38.8%, leading to high ductility, 16%, and low strength, UTS of 932 MPa. The microstructure near the end of $\alpha + \beta \rightarrow \beta$ phase transformation transformed to a soft phase.
3. The heat treatment cycles greatly affected the diffusion of alloying elements out of α and β phases.

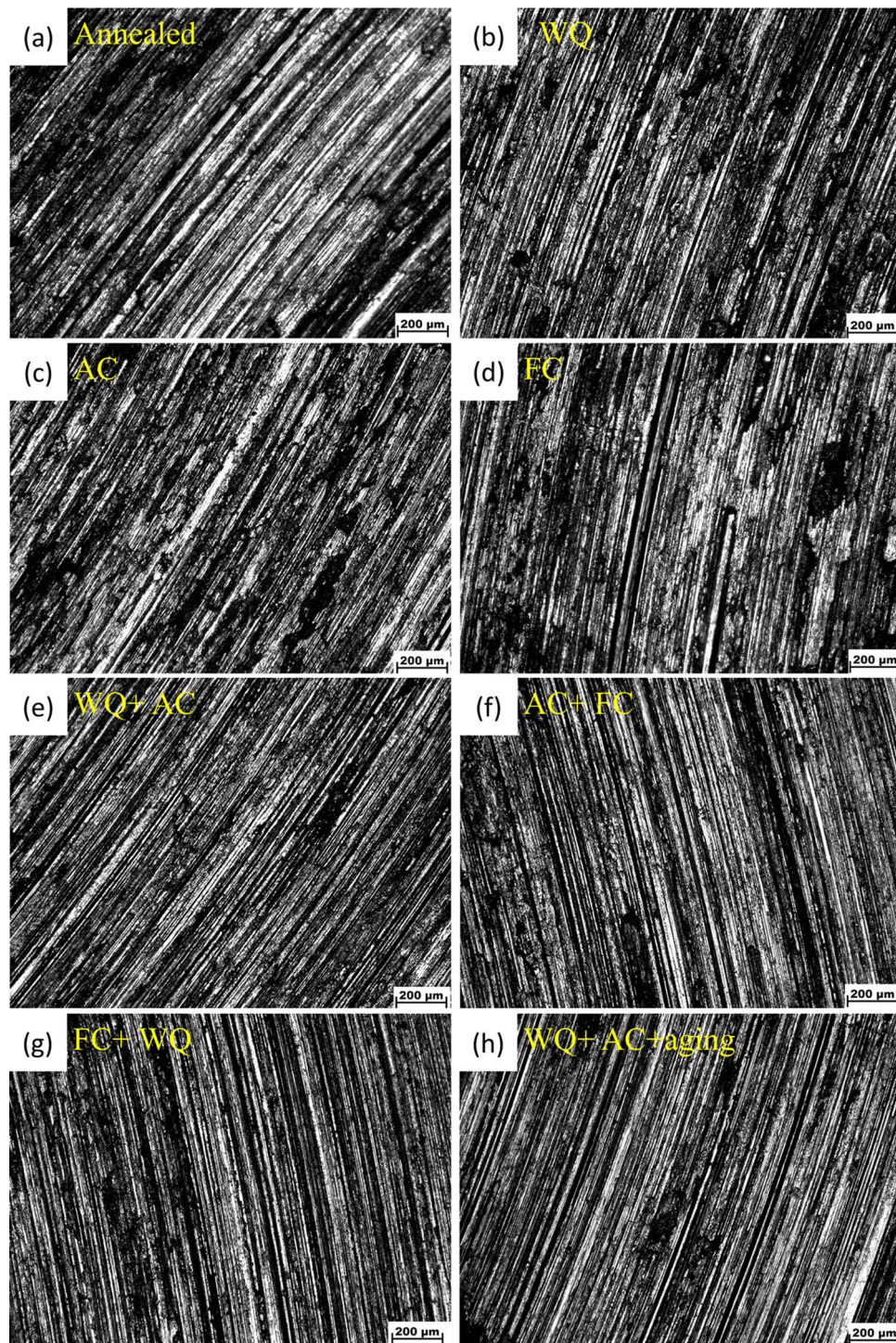


Fig. 11 Optical images of (a) annealed, (b) WQ, (c) AC, (d) FC, (e) WQ + AC, (f) AC + FC, (g) FC + WQ, (h) WQ + AC + aging, (i) AC + FC + aging, and (j) FC + WQ + aging Ti-6Al-7Nb alloy

4. The coefficient of friction increased with the hardness increase. Thermally treated Ti-6Al-7Nb alloys showed no significant variation in the CoF; the range of CoF was 0.38-0.41 for the hardness range of 344-364 HV. The

variation in CoF can be attributed to the amount of α phase and, hence, the hardness of the alloy.

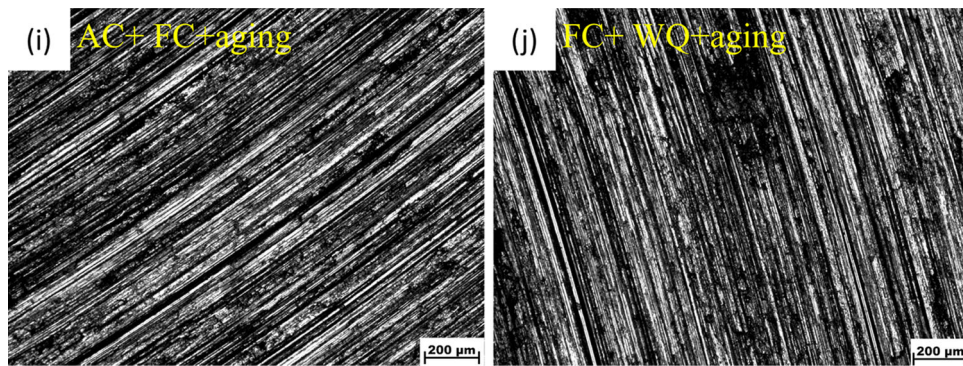


Fig. 11 continued

Acknowledgments

Author Shima El-Hadad would like to acknowledge the partial support from project No. 5540, Science Technology and Development Fund, STDF.

Funding

Open access funding provided by The Science, Technology & Innovation Funding Authority (STDF) in cooperation with The Egyptian Knowledge Bank (EKB).

Conflict of interest

The authors declare no conflict of interest.

Open Access

This article is licensed under a Creative Commons Attribution 4.0 International License, which permits use, sharing, adaptation, distribution and reproduction in any medium or format, as long as you give appropriate credit to the original author(s) and the source, provide a link to the Creative Commons licence, and indicate if changes were made. The images or other third party material in this article are included in the article's Creative Commons licence, unless indicated otherwise in a credit line to the material. If material is not included in the article's Creative Commons licence and your intended use is not permitted by statutory regulation or exceeds the permitted use, you will need to obtain permission directly from the copyright holder. To view a copy of this licence, visit <http://creativecommons.org/licenses/by/4.0/>.

References

1. E. de Santos Monteiro, F.M. de Souza Soares, L.F. Nunes, A.I. Carvalho Santana, R.S. de Biasi, and C.N. Elias, Comparison of the Wettability and Corrosion Resistance of Two Biomedical Ti Alloys Free of Toxic Elements with Those of the Commercial ASTM F136 (Ti-6Al-4V) Alloy, *J. Mater. Res. Technol.*, 2020, **9**, p 16329–16338.
2. I. Nedelchev, D. Veselinov, and H. Skulev, A Study of Anodizing of Ti-6Al-7Nb Alloy, in *2019 16th Conference on Electrical Machines, Drives and Power Systems*, IEEE, 2019, pp 1–6
3. A. Keshitta and M.A.-H. Gepreel, Effect of Sn-Addition on the Properties of the Biomedical Ti-17Nb-6Ta Alloy, *IOP Conf. Ser. Mater. Sci. Eng.*, 2019, **553**, p 12032.
4. A.M. Keshitta, M.A. Gepreel, and M. Abdel-Hady Gepreel, Shape Memory Effect in New Ti-Nb-Ta Alloy, in *Materials Science Forum*, Trans Tech Publications Ltd, 2017, pp 165–170
5. A.H. Awad and M. Abdel-Hady Gepreel, Basic Characterization of New Ti-Mn-Zr Alloys, *Mater. Today Proc.*, 2020, **33**, p 1904–1908.
6. A. Zaki, S. El-Hadad, and W. Khalifa, Surface Modification Effects on Microstructure and Mechanical Properties of Bio-Titanium Alloys, in *Materials Science Forum*, Trans Tech Publications Ltd, 2017, pp 199–204
7. A. Zaki, S. El-Hadad, and W. Khalifa, Assessment of Tribological Properties of Cast and Forged Ti-6Al-7Nb and Ti-6Al-4V Alloys for Dental Applications, in *TMS 2016 145th Annual Meeting & Exhibition: Supplemental Proceedings*, Springer, 2016, pp 693–700
8. J. Ran, F. Jiang, X. Sun, Z. Chen, C. Tian, and H. Zhao, Microstructure and Mechanical Properties of Ti-6Al-4V Fabricated by Electron Beam Melting, *Crystals*, 2020, **10**, p 972.
9. C. Leyens and M. Peters, *Titanium and Titanium Alloys: Fundamentals and Applications*, John Wiley & Sons, Hoboken, 2003
10. G. Lütjering and J.C. Williams, *Titanium*, Springer Science & Business Media, Cham, 2007
11. X. Fan, Q. Li, A. Zhao, Y. Shi, and W. Mei, The Effect of Initial Structure on Phase Transformation in Continuous Heating of a TA15 Titanium Alloy, *Metals (Basel)*, 2017, **7**, p 200.
12. B. Pazhanivel, P. Sathiyaraj, and G. Sozhan, Ultra-Fine Bimodal ($\alpha + \beta$) Microstructure Induced Mechanical Strength and Corrosion Resistance of Ti-6Al-4V Alloy Produced via Laser Powder Bed Fusion Process, *Opt. Laser Technol.*, 2020, **125**, 106017
13. M. Ashida, M. Hanai, P. Chen, and T. Hanawa, Developing Microstructure and Enhancing Strength of Ti-6Al-7Nb Alloy with Heat Treatment Processed by High-Pressure Torsion, *Mater. Trans.*, 2022, **63**, p 948–956.
14. B. Li, P. Ji, B. Chen, F. Wang, W. Ma, X. Zhang, M. Ma, and R. Liu, The Effect of Zr Addition on the Microstructure Evolution and Mechanical Properties of Hot-Rolled TiAlNbZr Alloy, *Mater. Sci. Eng. A*, 2021, **828**, 142114
15. C. Xu, F. Sikan, S.E. Atabay, J.A. Muniz-Lerma, O. Sanchez-Mata, X. Wang, and M. Brochu, Microstructure and Mechanical Behavior of As-Built and Heat-Treated Ti-6Al-7Nb Produced by Laser Powder Bed Fusion, *Mater. Sci. Eng. A*, 2020, **793**, 139978
16. M.S. Kalienko, A.V. Zhelnina, A.V. Volkov, and P.E. Panfilov, Thermal Stability of Ti6242S and Ti-6Al-7Nb Alloys, *Russ. Metall.*, 2022, **2022**, p 1211–1217.
17. ASTM International Committee E37 on Thermal Measurements, *Standard Test Method for Linear Thermal Expansion of Solid Materials with a Push-rod Dilatometer1*, ASTM International, 2017
18. A.G. Illarionov, F.V. Vodolazskiy, N.A. Barannikova, Y.I. Kosmatskiy, and Y.V. Khudorozhkova, Influence of Phase Composition on Thermal Expansion of Ti-04Al, Ti-22Al-25Zr and Ti-3Al-25V Alloys, *J. Alloys Compd.*, 2021, **857**, 158049
19. L. Bolzoni, T. Weissgaerber, B. Kieback, E.M. Ruiz-Navas, and E. Gordo, Mechanical Behaviour of Pressed and Sintered CP Ti and Ti-6Al-7Nb Alloy Obtained from Master Alloy Addition Powder, *J. Mech. Behav. Biomed. Mater.*, 2013, **20**, p 149–161.
20. M.J. Donachie, *Titanium: A Technical Guide*, ASM international, 2000
21. A.H. Awad, H.A. El-Hofy, A. Chiba, and M.A.-H. Gepreel, Robust Mechanical Properties and Corrosion Resistance of New Low-Cost Hot-Forged and Aged β -type Ti-14Mn-(x)Zr Alloys, *J. Alloys Compd.*, 2022, **904**, 164098

22. R.K. Gupta, V.A. Kumar, and S. Chhangani, Study on Variants of Solution Treatment and Aging Cycle of Titanium Alloy Ti6Al4V, *J. Mater. Eng. Perform.*, 2016, **25**, p 1492–1501.
23. A. Shaikh, S. Kumar, A. Dawari, S. Kirwai, A. Patil, and R. Singh, Effect of Temperature and Cooling Rates on the $\alpha+\beta$ Morphology of Ti-6Al-4V Alloy, *Procedia Struct. Integr.*, 2019, **14**, p 782–789.
24. I. Hulka, N.R. Florido-Suarez, J.C. Mirza-Rosca, and A. Saceleanu, Mechanical Properties and Corrosion Behavior of Thermally Treated Ti-6Al-7Nb Dental Alloy, *Materials (Basel)*, 2022, **15**, p 3813.
25. R. Reda and A. Adel, Heat Treatment of Low Cost Beta Titanium Alloy Produced by Investment Casting, *J. Pet. Min. Eng.*, 2020, **22**, p 35–41.
26. Y. Oshida, *Bioscience and Bioengineering of Titanium Materials*, Elsevier, Amsterdam, 2010
27. Y. Guo, S. Wei, S. Yang, Y. Ke, X. Zhang, and K. Zhou, Precipitation Behavior of ω Phase and $\omega \rightarrow \alpha$ Transformation in Near β Ti-5Al-5Mo-5V-1Cr-1Fe Alloy during Aging Process, *Metals (Basel)*, 2021, **11**, p 273.
28. X. Shi, W. Zeng, and Q. Zhao, The Effects of Lamellar Features on the Fracture Toughness of Ti-17 Titanium Alloy, *Mater. Sci. Eng. A*, 2015, **636**, p 543–550.
29. M. Fella, M. Labaiz, O. Assala, L. Dekhil, A. Taleb, H. Rezag, and A. Iost, Tribological Behavior of Ti-6Al-4V and Ti-6Al-7Nb Alloys for Total Hip Prosthesis, *Adv. Tribol.*, 2014 <https://doi.org/10.1155/2014/451387>
30. M.H. Kim, K.Y. Rhee, Y.N. Paik, J.S. Hong, and Y.S. Ham, Experimental Investigation on the Mechanical Behavior of High-Frequency Induction-Hardened Mild Carbon, SPS5 Steel, *Mater. Sci. Eng. A*, 2008, **485**, p 31–38.
31. D. Odabas, The Influence of the Temperature on Dry Friction of AISI 315 Steel Sliding Against AISI 3150 Steel, in *IOP Conference Series: Materials Science and Engineering*, IOP Publishing, 2018, p 12021

Publisher's Note Springer Nature remains neutral with regard to jurisdictional claims in published maps and institutional affiliations.